ACS APPLIED MATERIALS & INTERFACES

www.acsami.org

Research Article

Self-Assembled Plasmonic Structural Color Colorimetric Sensor for Smartphone-Based Point-Of-Care Ammonia Detection in Water

Mahdi Soudi, Pablo Cencillo-Abad, Jay Patel, Suvash Ghimire, Joseph Dillon, Aritra Biswas, Kausik Mukhopadhyay, and Debashis Chanda*

Cite This: https://doi.org/10.1021/acsami.4c06615

Read Online

ACCESS | Metrics & More | Article Recommendations | Supporting Information

ABSTRACT: Monitoring chemical levels is crucial for safeguarding both the environment and public health. Elevated levels of ammonia, for instance, can harm both humans and aquatic ecosystems, often indicating contamination from agriculture, industry, or sewage. Developing portable, high-resolution, and affordable methods for in situ monitoring of ammonia is thus imperative. Plasmonic sensors offer a promising solution, detecting ammonia by correlating changes in their optical response to the target analyte's concentration. While they are highly sensitive and can be fabricated in a variety of portable and user-friendly formats, some still require reagents or expensive optical equipment, which hinder their widespread adoption. Here, we present a self-assembled nanoplasmonic colorimetric sensor capable of directly detecting ammonia concentrations in aqueous matrices. The proposed sensor exploits the plasmonic resonance of the nanostructures to transduce changes in the chemical environment into alterations in color, offering a label-free method for real-time analysis. The sensor is fabricated using a self-assembling technique compatible with low-cost mass production based on aluminum and aluminum oxide, ensuring affordability and avoiding the use of other toxic chemicals. We developed a model to predict ammonia concentrations based on visible color change of the sensor, achieving a detection limit of 8.5 ppm. Furthermore, to address the need for on-site detection, we integrated smartphone technology for real-time color change analysis, eliminating the need for expensive, bulky optical instruments. Indeed, our approach offers a cost-effective, portable, and user-friendly solution for ammonia detection in water without the need for chemical reagents or spectrometers, making it ideal for field applications. Interestingly, this platform extends its applicability beyond ammonia detection, enabling the monitoring of various chemicals using a smartphone, without the need for any additional costly equipment.

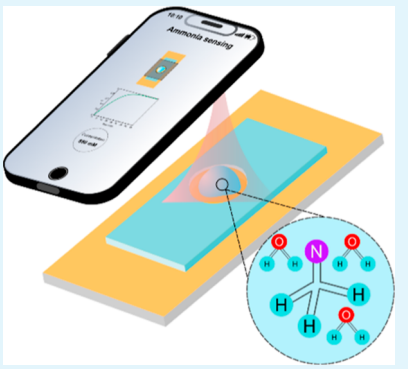

KEYWORDS: *nanosensors, colorimetric sensors, aqueous ammonia sensing, structural color, self-assembled*

INTRODUCTION

Among many chemicals, monitoring ammonia concentrations in water sources is vital for environmental protection and public health. Elevated ammonia levels in water pose human health risks, causing gastrointestinal and respiratory issues upon ingestion, as well as skin and eye irritation through direct contact.[1−3] Moreover, ammonia pollution in aquatic systems can lead to increased acidity, toxicity, and eutrophication,[4,5] negatively affecting aquatic organisms' survival, growth, and reproduction, and thus disrupting the ecosystem equilibrium.[6] Finally, ammonia monitoring in water is also crucial for pollution prevention, as high ammonia concentrations in water often indicate contamination from agricultural runoff, as well as industrial and sewage effluents.[7] Recognizing these harmful impacts, the Department of Human Services sets environmental limits for ammonia in US surface water ranging from 0.25 to 32.5 ppm.[8] In sum, effective water resource management requires practical and reliable methods for assessing waterborne ammonia levels to safeguard aquatic ecosystems, ensure potable water quality, and mitigate potential health hazards.[9,10]

Conventional methods of detection of ammonia in water are typically classified as electrochemical, biological, and optical.[9,11] Electrochemical sensors for ammonia detection use ion-selective electrodes that are sensitive to the presence of ammonia ions. These sensors translate changes in electrical properties such as voltage, conductivity, or current flow into ammonia concentrations.[11,12] While they offer an affordable and versatile solution for fast in situ measurements, they require calibration and can be affected by interfering species.[12,13] In contrast, biological methods excel in ammonia detection when high specificity is required. For instance, enzyme-based approaches trigger an ultraselective biological reaction upon enzyme−analyte interaction, yielding data that is then transformed into a quantifiable and interpretable electrical

Received: April 22, 2024
Revised: August 6, 2024
Accepted: August 7, 2024

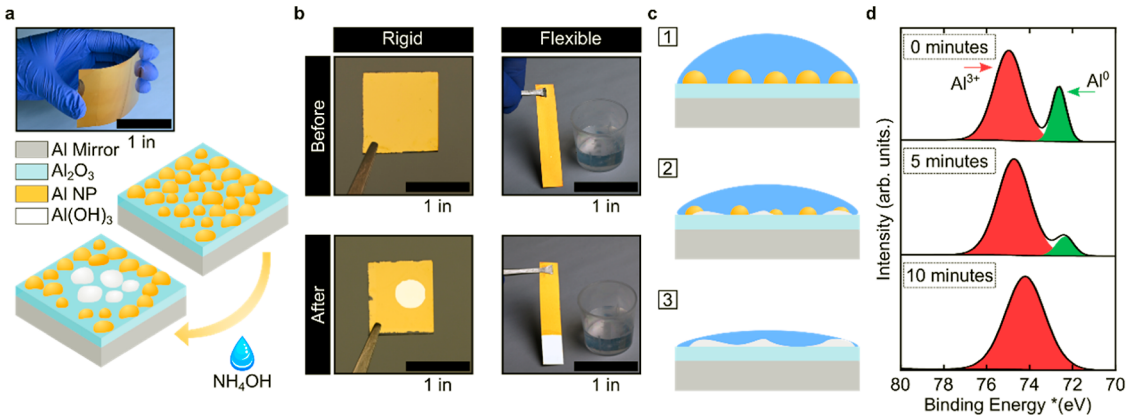

Figure 1. Chemical reaction-induced color change in nanosensor. (a) The plasmonic colorimetric sensor consists of an aluminum self-assembled layer on top of a thin Al_2O_3 layer over a back mirror on rigid (glass) and flexible (PET) substrates. (b) Nanoislands structural change causes observable color shifts before/after exposure to dissolved ammonia in water. (c) Al_2O_3 transforms to Al $(OH)_3$ after reaction with dissolved ammonia in water. Subsequent exposure to water prompts Al_2O_3 layer formation, cyclically. (d) XPS measurements of the top surface of the sensor at different time intervals show a decrease in aluminum metal peak and an increase in aluminum hydroxide peak, indicating that aluminum nanoparticles oxidize during the reaction with aqueous ammonia.

or optical signal via an associated physical or chemical transducer.[14−16] However, despite delivering precision, these methods necessitate intricate sample preparation and entail higher costs. Alternatively, optical detection methods harness the optical attributes of substances to conduct chemical analyses, demonstrating portability, cost-effectiveness, and high resolution.[17−19] Among all optical detection methods, surface-enhanced Raman scattering has drawn attention due to its low limit of detection (1 ppm), high response time (within a few seconds), and high sensitivity.[20,21] In addition, colorimetric or fluorescent reagents are introduced into the target solutions to interact with ammonia, inducing alterations in color or fluorescence that are directly correlated to the ammonia concentration.[22,23] Among these, the Indophenol Blue (IPB) method, a colorant-based approach, and the *o*-phthalaldehyde (OPA) method, a fluorant-based approach, stand as the two prevailing methods.[24−27] Notably, while the OPA method is more sensitive, the IBP method offers a simpler and more inexpensive solution. This makes the IBP method the standard choice for determining ammonia in water by the U.S. Environmental Protection Agency,[28] highlighting the need for developing further methods that not only deliver high resolution but also ensure the necessary portability and cost-effectiveness.

The widespread use of nanofabrication techniques over the past decades has enabled the development of plasmonic structures for chemical sensing.[29−31] When light of a specific wavelength illuminates a metallic nanostructure, it induces a collective and coherent oscillation of the free electrons within the metal, a phenomenon known as plasmon resonance. These oscillations result in subwavelength areas of high-density electromagnetic fields that are extremely sensitive to their surroundings. These hotspots can detect the presence of subwavelength chemical compounds, as the resonant wavelength of light interacting with the metal nanostructure changes when the chemical compound is present nearby.[32] This unique combination of compact, high-resolution, and real-time detection has spurred researchers to develop plasmonic sensors for a variety of applications, ranging from environmental monitoring to medical diagnostics.[33−36] In recent years, various plasmonic architectures have been proposed for the determination of ammonia concentration in aqueous matrices.[37−44] However, all these techniques lack portability and user-friendliness, as they still rely on the use of reagents or expensive optical equipment like spectrometers, which prohibits their potential for widespread adoption.[45]

Here, we present a low-cost, easy-to-use, and label-free plasmonic colorimetric sensor that detects ammonia in water by correlating the color change in the sensor with the concentration of the target solution. The plasmonic structure consists of a self-assembled layer of aluminum nanoparticles on an aluminum backplane coated with a thin transparent oxide supporting gap plasmons at visible wavelengths.[46] Hence, when illuminated by surrounding white light, the nanostructure absorbs certain spectral bands and reflects the rest, resulting in a specific color appearance. Interestingly, when the aluminum nanoparticles interact with ammonia in water, the nanoparticles oxidize, leading to a loss of color. Thus, by analyzing this color transformation, the concentration of ammonia can be determined directly from the solution without the need for any additional reactants. Importantly, this colorimetric platform relies on a self-assembling technique for the production of large-scale and low-cost structural color fully compatible with industrial standards, allowing thus for a cost-effective and high-volume production method for the sensors, essential for commercial success.[46−48] Finally, we show how a simple algorithm that uses a smartphone camera and image recognition can eliminate the need for traditional bulky and expensive spectroscopic systems, simplifying the color-reading process. Our colorimetric plasmonic platform only requires a sensor and a smartphone to determine ammonia levels as low as 8.5 ppm in water, eliminating the need for additional chemicals or costly equipment. This makes the sensor suitable for use in contexts where low cost and portability are required.

RESULTS AND DISCUSSION

Plasmonic Sensor. Although many plasmonic structures have been proposed for chemical and ammonia detection in recent years, they often use complex lithography-based fabrication methods, costly noble metals, such as gold or silver, and need optical equipment like spectrometers, that impede scalability and hamper their potential for application

https://doi.org/10.1021/acsami.4c06615
ACS Appl. Mater. Interfaces XXXX, XXX, XXX−XXX

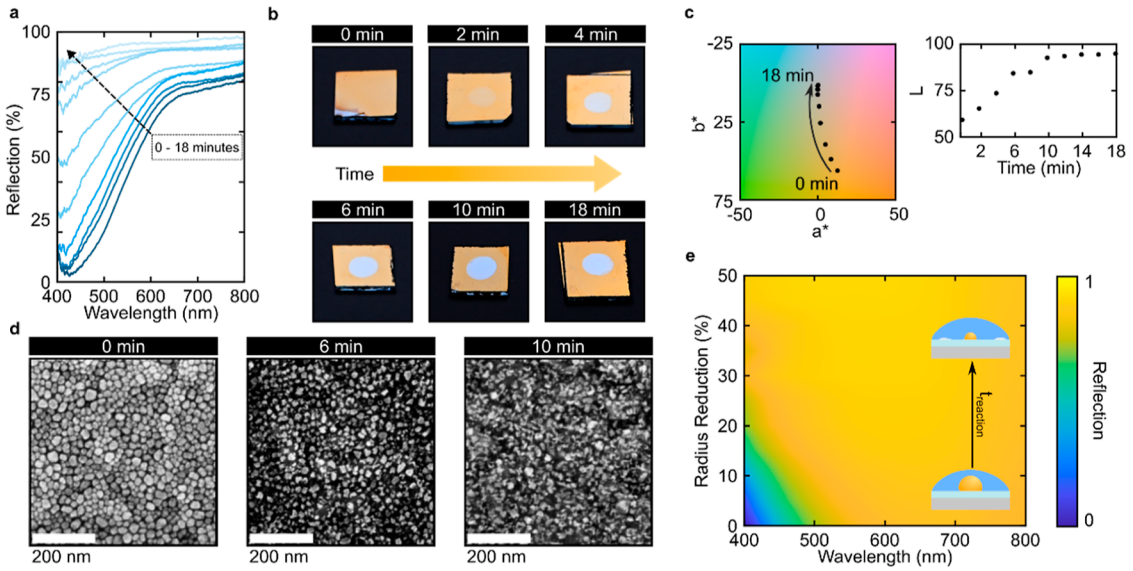

Figure 2. Time-dependent color shift. (a) The reflection curve of the sensor as it reacts with dissolved ammonia in water at a concentration of 1 mM. (b) Optical images of the sensor at various time intervals after reacting with dissolved ammonia in water (c) the corresponding color shift is shown on CIELAB space. (d) SEM images of the sensor at various time intervals after reacting with dissolved ammonia in water. (e) simulation of reflection curves for varying time intervals during which the radius of the nanoislands reduces.

beyond proof-of-principle demonstrations. In contrast, here we propose a plasmonic colorimetric platform that is based on inexpensive aluminum and fabricated with large-scale self-assembling. Specifically, the nanostructure is fabricated by sequentially evaporating, on an e-beam evaporator, an optically thick layer of aluminum (100 nm), a thin layer of aluminum oxide (10 nm), and a self-assembly layer of aluminum nanoparticles (4.5 nm).[49] The schematic of the proposed sensor is shown in Figure 1a. Interestingly, when coupled to the ambient light, the free electrons in the metal nanoparticles oscillate collectively, resulting in plasmon resonances. In our structure, for spectral components of light matching the plasmon resonance, strong absorption occurs, while off-resonance components are reflected by the aluminum mirror, ultimately producing vibrant colors. Due to the plasmonic self-assembly's proximity to the back mirror, the electromagnetic mode is coupled to the ultrathin cavity, making it extremely sensitive to environmental changes while remaining relatively angle and polarization-independent. Given that the nanostructure color results from subtracting certain bands, corresponding to the plasmon resonances, from incident white light, if the resonance condition changes due to alterations in the environment or the nanostructure's geometry, the color will also change.[47,49] Thus, if aqueous ammonia interacts with the nanoparticles, changing their geometry or material properties, it will result in color changes that can be exploited for concentration determination.

As a result, when a solution containing dissolved ammonia in water is applied to the sensor's surface, the sensor's color changes due to the surface oxidation of the aluminum nanoparticles. This oxidation reaction alters the metallic properties of the nanoparticles, consequently disrupting the plasmon resonance and leading to a change in color, with the reaction rate serving as an indicator of the ammonia concentration in the water sample. Hence, by analyzing the time-dynamics of the color changes in the nanostructure, we can determine the concentration of the solution. In the following section, we will describe the chemistry of the reaction, discuss the physical and optical foundations of the detection mechanism, and present a theoretical model for correlating the color change dynamics with the ammonia concentration. Finally, we will demonstrate how this characterization, traditionally conducted through spectroscopic analysis, can be substituted with color analysis using a smartphone camera and a simple image recognition algorithm, providing a practical, cost-effective, and in situ platform for ammonia detection in aqueous matrices.

Chemistry of the Reaction. When exposed to air, aluminum nanoparticles rapidly develop a thin layer of aluminum oxide. This passivation layer shields aluminum from further oxidation in various environments, such as water, organic solvents, and biological systems, allowing a nanosensor to be submerged in water without losing its color. However, when low concentrations of ammonia are added to the water at room temperature, the aluminum oxide layer reacts with ammonium hydroxide, leading to the formation of aluminum hydroxide ($Al(OH)_3$) as a white insoluble precipitate

$$Al_2O_3 + 3NH_4(OH) \rightarrow 3NH_3 + 2Al(OH)_3 \quad (1)$$

As a result of this chemical reaction, the aluminum core of the nanoparticles is exposed to the water, facilitating interaction and the subsequent formation of aluminum hydroxide until the reaction is completed

$$2Al + 6H_2O \rightarrow 2Al(OH_3) + 3H_2 \quad (2)$$

As the reaction progresses, the nanoparticles reduce in size and change shape. Consequently, the plasmonic response responsible for the optical absorption is lost, causing the color to shift from saturated yellow to white, Figure 1b,c. To further validate the proposed chemical mechanism, XPS measurements were conducted on sensors before and after 5 and 10 min of interaction with a 1 mM concentration of ammonia in water (see Supporting Information). Indeed, XPS measurements show how, over time, the area under the peak corresponding to aluminum metal (Al^0) decreases while the

https://doi.org/10.1021/acsami.4c06615
ACS Appl. Mater. Interfaces XXXX, XXX, XXX−XXX

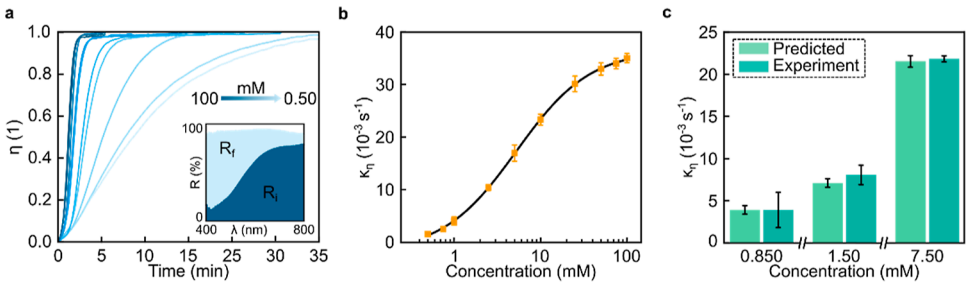

Figure 3. Reflection spectra-based sensor calibration. (a) Time dynamic response for concentrations ranging from 0.5 to 100 mM. (b) Applying the Logistic function fit to κ_η for the same concentration in (a) to develop a model for predicting κ_η for unknown concentrations. (c) Comparing the predicted values obtained from the model in (b) to the experimental values of the reaction growth rate. The error bars in the predicted data set represent the propagation of uncertainty from the model in (b), while the error bars in the experimental data set represent the standard deviation from the mean.

area under the peak corresponding to the oxidized states (Al^{3+}) increases, Figure 1d.

Ammonia-Induced Color Transformation. The precise change in the sensor's color can be determined by collecting its reflection spectrum during the reaction of aluminum nanoparticles with ammonia in water. To achieve this, we dropcast 50 μL of 1 mM aqueous ammonia onto the sensor at room temperature while simultaneously recording the reflection spectrum using an optical spectrometer (see Methods). Figure 2a shows reflection measurement taken every 90 s, with the first and last curves corresponding to the reflectance response at the beginning and after 18 min of the reaction, respectively. As expected, the oxidation of aluminum nanoparticles by aqueous ammonia significantly impacts the optical resonance, gradually diminishing the reflection dip until it resembles the flat curve characteristic of a simple aluminum mirror by the 18-min mark, Figure 2b. This loss of color can be better appreciated when converting the reflection measurements into CIELAB color space, Figure 2c. This color space is a three-dimensional model defined by three values: L (lightness) ranging from 0 to 100, a representing the position on the green-to-red axis, and b representing the position on the blue-to-yellow axis. CIELAB is device-independent and defined based on standard illuminants (e.g., D65) and standard observer functions.[50] This ensures that the color values remain consistent regardless of the color measurement instrument as long as the measurement is made under the same illuminant and observer conditions. Interestingly, among all three parameters, the lightness displays the most remarkable behavior, with a monotonically increasing trend until saturation close to L = 100. This observation will be utilized later in the development of the smartphone-based recognition platform.

To gain a deeper understanding on the mechanism of color change, we acquired SEM micrographs of the sensor at three stages: before interaction, after 6 min of interaction, and after 10 min, Figure 2d. The changes are consistent with our previous assessment. Oxidation not only changes the material properties but also dissolves the nanoparticles. To investigate the effect of this morphological change in the optical response of the sensor, we performed FDTD simulations, Figure 2e. To simplify the simulation requirements, we chose a single nanoparticle with periodic boundary conditions and plane-wave illumination at normal incidence. Mimicking the behavior observed in the SEM analysis, we performed a series of simulations with the particle size being reduced from 100 to 50% of its original size, as obtained from the statistical analysis of the particles in the sensor before interacting with aqueous ammonia. As shown in measure spectra in Figure 2a and UV–vis spectrophotometric analysis shown in Figure S5, as the particle size is reduced, the original gap-plasmon resonance around λ = 420 nm, which gives the characteristic yellow color of the sensor shifts toward UV, resulting in a flatter response in the visible part of the spectrum until an almost featureless plot is recovered, corresponding to the white mirror-like appearance when no plasmons can be excited anymore.

Sensor Calibration. In order to use the proposed nanosensor to determine the concentration of the solution, we need to correlate the changes in the reflection spectrum, i.e. the color appearance of the sensor, to the concentration of the ammonia in water. To study the changes in the sensor's reflection spectrum as it interacts with aqueous ammonia in more detail, we aim to quantify these changes using a parameter denoted as η. This parameter, referred to as the sensor's time dynamic response, is calculated by integrating the difference between the reflection spectra at a given time, $R(t)$, and the initial time, $R(t_0)$. To normalize the η value to a range between 0 and 1, we divide it by the wideband of the visible spectrum.

$$\eta = \frac{\int_{400}^{800} [R(t) - R(t_0)]\mathrm{d}\lambda}{\int_{400}^{800} \mathrm{d}\lambda} \tag{3}$$

To monitor the dependency of η on the concentration of ammonia, we conducted a series of experiments with concentrations ranging from 0.50 to 100 mM ammonia and obtained η corresponding to each concentration (see Methods). For accurate η values, we conducted the experiment a minimum of five times, subsequently calculating the mean value and associating the appropriate statistical error. As can be seen in Figure 3a, variations in concentration influence the reaction speed and, thus, the sensor's time dynamic response. The observed variations in η due to changes in concentration, which impact reaction speed, indicate that the sensor's time dynamic response is highly sensitive to concentration changes. Therefore, the sensor's time dynamic response can effectively be used for calibrating the sensor to determine the concentration of unknown solutions. Accordingly, we aim to derive a singular parameter capable of characterizing the time dynamic response of the sensor. Because the sensor response curves resemble a sigmoid function, Figure 3a, we choose to fit the Gompertz function, which is a special case of a sigmoid function, to the experimental curves and extract the reaction

https://doi.org/10.1021/acsami.4c06615
ACS Appl. Mater. Interfaces XXXX, XXX, XXX−XXX

growth rate, κ_η, for each concentration. The Gompertz function takes the form

$$\eta(t) = ae^{-be^{-\kappa t}} \tag{4}$$

where a is the upper asymptote, representing the maximum value the dependent variable can attain, b is a constant that influences the horizontal position or shift of the curve along the x-axis, and κ is the reaction growth rate, influencing the steepness of the curve (see Supporting Information).

In good agreement with our observation and interpretation from the time dynamic response of the sensor to different concentrations of aqueous ammonia, the reaction growth rate increases as the concentration increases, Figure 3b. The sensor can be calibrated by leveraging the similarity between the dependence of reaction growth rate on concentration and the behavior described by the Logistic function[51]

$$\kappa_\eta = A_2 + \frac{A_1 - A_2}{1 + \left(\frac{c}{c_0}\right)^p} \tag{5}$$

where A_1 and A_2 are the upper and lower limits of the variable, c represents the concentration, c_0 is the concentration value where the curve reaches the midpoint between A_1 and A_2, and p is a parameter that controls the curve's slope.

The obtained calibration curve in Figure 3b can be used to predict the value of κ_η for any concentration. To obtain the predicted value for any desired concentration, the concentration value (c) in eq 3 can be replaced by any concentration. The calculated κ_η will be specific to the inserted concentration. To determine the concentration for any unknown solution by using the proposed method, we have developed an algorithm that can be used to determine the concentration of the unknown solution by using changes in the reflection spectrum. For this purpose, the user can record the reflection spectrum of the sensor while enough amount of the solution has been dropped on the sensor (see Methods). In computing the κ_η for the test solution, the algorithm uses the sensor's reflection spectrum during its interaction with the solution. This facilitates the acquisition of η values at different time intervals. It is worth noting that the time intervals between recordings depend on the solution's concentration. Higher concentrations result in faster reaction rates, leading to quicker changes in the reflection spectrum. This necessitates shorter time intervals compared to lower concentrations, ensuring an ample amount of data for precise computation of the reaction growth rate. Once the algorithm obtained the values for η, the reaction growth rate for the test solution can be determined by using the Gompertz function. Afterward, the algorithm substitutes the κ_η value in eq 5 and predicts the concentration.

To validate the proposed algorithm and calibration curve, we intend to obtain both experimental and predicted values of κ_η for three different test concentrations of aqueous ammonia: 0.85, 1.50, and 7.50 mM. The predicted value of κ_η can be obtained from eq 4, where error bars are calculated from error propagation

$$\Delta\kappa_\eta = \sqrt{\left(\frac{\partial\kappa_\eta}{\partial A_1}\Delta A_1\right)^2 + \left(\frac{\partial\kappa_\eta}{\partial A_2}\Delta A_2\right)^2 + \left(\frac{\partial\kappa_\eta}{\partial p}\Delta p\right)^2} \tag{6}$$

where ΔA_1, ΔA_2 and Δp represent the uncertainty values of the variables. For the experimental values, we conducted experiments for each of these concentrations to determine the experimental κ_η values. To enhance the reliability of the measurement results, we performed the experiment five times for each concentration. These repetitions enabled us to calculate the mean value and its corresponding standard deviation, which represents the statistical error associated with the measurements. Comparing predicted and experimental values in Figure 3c, we can see the clear agreement between the two data sets.

Smart Phone-Based Concentration Detection. The use of a spectrometer, as explained in the previous section, is expensive and also poses challenges for onsite detection. To enhance the portability and usability of the proposed sensor, we can leverage the smartphone's camera and computing capabilities in combination with our colorimetric sensing platform to replace the need for such a system. We developed an algorithm that detects the color change during the reaction and determines the test solution's concentration using user-recorded videos while the nanoparticles react with ammonia in water, Figure 4a. This algorithm captures snapshots every 5 seconds as the nanoparticles' size decreases and the sensor's color changes. Subsequently, the algorithm calculates the average RGB value for each snapshot and converts them into the CIELAB color space parameters (see Methods). As mentioned earlier, within the CIELAB color space, we specifically utilize the lightness parameter (L) to effectively track color variations over time. We made this choice based on its significant responsiveness to changes in sensor coloration, which enables precise determination of the test solution's concentration using image recognition, Figure 4b.

To determine the concentration of aqueous ammonia using smartphone-recorded video, we need initial data to train the algorithm to correlate color changes with concentration. To

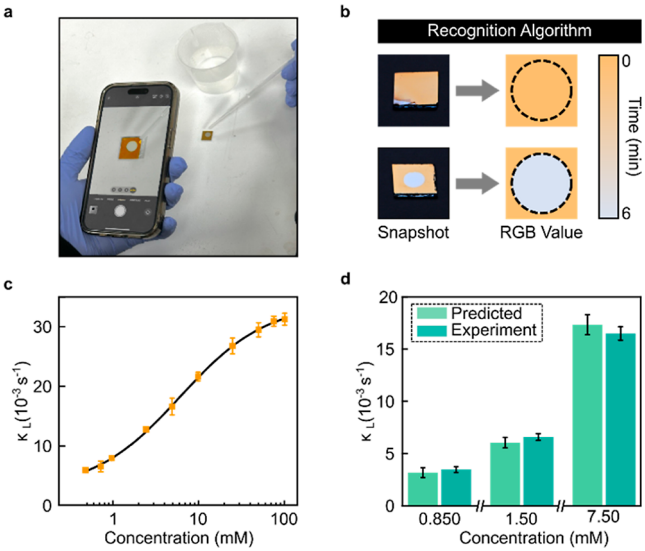

Figure 4. Smartphone-based chemical concentration prediction. (a) A smartphone can be used to determine the concentration of aqueous ammonia. (b) The algorithm for determining concentration using a smartphone. (c) Applying the Logistic function fit to the κ_L to develop a model for predicting κ_L for unknown concentrations. (d) Comparing the predicted values obtained from the model in (c) to the experimental values of κ_L for concentrations. The error bars in the predicted data set represent the propagation of uncertainty from the model in (c), while the error bars in the experimental data set represent the standard deviation from the mean.

https://doi.org/10.1021/acsami.4c06615
ACS Appl. Mater. Interfaces XXXX, XXX, XXX−XXX

accomplish this, we convert the reflection spectrum recorded in the previous section into the CIELAB color space. To monitor the changes of lightness as the concentrationn is changing, we extracted the value of the lightness corresponding to each time step and analyzed the changes in the lightness as time passed. Interestingly, we observed the same behavior of η in the previous section. Therefore, we used the same Gompertz function again to fit the lightness values of each concentration. Consequently, we obtained the reaction growth rate based on the lightness (κ_L) and by plotting the κ_L of each concentration versus concentration in Figure 4c, we observe a similar behavior to κ_η. As before, we can define a calibration curve by fitting to the Logistic function. To validate our detection method, we compare the sensor's response values predicted from the calibration curve to the ones determined by the smartphone detection platform explained earlier. The smartphone camera records a video capturing the interaction of three concentrations (0.85, 1.50, and 7.5 mM) with the nanosensor, allowing us to extract the color change in the region of interest. Using the approach described above, we can then determine the experimental values of κ_L. Figure 4d shows the agreement between these experimental values and those predicted by the calibration curve, validating the accuracy of the smartphone-based detection platform under real experimental conditions. The error bars in the experimental data set represent the standard deviation around the mean value, while those in the predicted data set are determined through error propagation. Remarkably, smartphone detection simplifies both data acquisition and processing while maintaining excellent detection sensitivity akin to the spectroscopic approach. Indeed, compared to conventional equipment (Figure 3c), the smartphone-based platform (Figure 4b) also enables the determination of submillimolar concentrations with comparable limits of detection of 8.50 ppm and a linear dynamic range from 8.5 to 1700 ppm. The sensor demonstrates a response time that varies from 3 to 30 min, depending on the concentration. Finally, the slope of the sensor's response curve (Figure 4d) within its linear range yields a sensitivity of approximately 0.87 s^{-1} M^{-1}.

CONCLUSION

In conclusion, we have introduced a self-assembled, easy-to-use, label-free, and cost-effective colorimetric plasmonic nanosensor designed for ammonia detection . The sensor's layered structure generates an enhanced gap plasmon mode with visible-range absorption, closely correlated with nanoparticle geometry. As a result, changes in nanoparticle configuration induced by their interaction with the solution produce a distinct color shift in the sensor, enabling its ammonia detection capabilities. To determine ammonia concentrations, we initially used variations in reflective spectra to establish a predictive model for the reaction growth rate. Our experiments demonstrated the agreement between predicted and measured values, affirming the method's effectiveness. Finally, recognizing the need for on-site portable aqueous ammonia detection, we eliminated the need for an optical spectrometer by leveraging the smartphone's imaging and analysis capabilities. To determine solution concentrations, our algorithm analyzed color changes during reactions by converting average RGB values extracted from user-recorded videos into the CIELAB color space and then tracks lightness changes over time. As a result, this model allows us to determine the concentration of solutions of ammonia in water through a low cost mean. Comparing predicted and experimental values obtained with our method demonstrates the platform's performance under real experimental conditions, highlighting its potential as a low-cost, portable, and easy-to-usefor ammonia detection in aqueous matrices without chemical reactants or spectrometers.

In contrast to conventional electrochemical, biological, and optical methods, our proposed sensor prioritizes affordability, nontoxicity, compactness, and ease of use based on smartphones. This enables point-of-care ammonia detection, making it a practical tool for real-world applications without the need for additional reagents, unlike other existing detection techniques. By utilizing a colorimetric sensing platform and a smartphone, this technique opens up a wide range of chemical detection applications: from safeguarding aquatic ecosystems through on-site ammonia monitoring in runoff water to supporting healthy agriculture by optimizing fertilizer use, this approach leverages the computational power of smartphones for a more sustainable future.

METHODS

Sensor Fabrication. The optically thick back mirror is produced by evaporating 100 nm of aluminum on an e-beam evaporator (AJA International) on top of glass and polyethylene terephthalate (PET) film for rigid and flexible sensors, respectively. A 10 nm spacer layer of aluminum oxide was then grown by atomic layer deposition (Savannah 200, Cambridge Nanotech) by pulsing trimethylaluminum and water at 100 °C. The aluminum nanoparticles were then self-assembled on the electron beam evaporator. To produce a yellow color, based on previous studies, we chose to grow 4.5 nm of aluminum nanoparticles.[49,52]

Solution Preparation. Ammonia solution [BioUltra, ~1 M NH_3 in H_2O(T)] was purchased from Sigma-Aldrich. To prepare the solution at various concentrations, we diluted the ammonia by adding deionized water. For this study, we prepared the following concentrations: (0.5, 0.75, 0.85, 1, 1.5, 3, 5, 7.5, 10, 12.5, 25, 50, 75, and 100 mM).

Experiment Protocol. To monitor the sensor's reflection spectrum changes during the reaction between aluminum nanoparticles, which is responsible for color, and dissolve ammonia in water, we incubate (50 μL) of the solution with the desired concentration onto the sensor at room temperature. To stop the solution from spreading over the sensor, we apply a thin layer of polydimethylsiloxane (PDMS). To prevent the ammonia from evaporating, we cover the PDMS surface with a transparent coverslip. We obtained reflection curves by directing unpolarized light at a normal angle of incidence onto the samples using a 4× objective lens with a 0.07 numerical aperture. These curves were then captured with a fiber-coupled spectrometer (HR 2000+, Ocean Optics). To normalize the measurements, we used an aluminum mirror as a reference.

Colorimetric Analysis. To convert the reflection spectrum of the sensor to CIELAB color space, we first calculate the XYZ tristimulus values integrating over the visible spectrum according to

$$X = \frac{1}{N}\int \bar{x}(\lambda)R(\lambda)I(\lambda)\mathrm{d}\lambda \tag{7}$$

$$Y = \frac{1}{N}\int \bar{y}(\lambda)R(\lambda)I(\lambda)\mathrm{d}\lambda \tag{8}$$

$$Z = \frac{1}{N}\int \bar{z}(\lambda)R(\lambda)I(\lambda)\mathrm{d}\lambda \tag{9}$$

$$N = \int \bar{y}(\lambda)I(\lambda)\mathrm{d}\lambda \tag{10}$$

https://doi.org/10.1021/acsami.4c06615
ACS Appl. Mater. Interfaces XXXX, XXX, XXX−XXX

where $R(\lambda)$ is the measured reflectance, $x(\lambda)$, $y(\lambda)$, and $z(\lambda)$ are color matching functions, and $I(\lambda)$ is the reference illuminant. CIELAB coordinates can be derived from the tristimulus values from

$$L = 116f_y - 16 \tag{11}$$

$$a = 500(f_x - f_y) \tag{12}$$

$$b = 200(f_y - f_z) \tag{13}$$

with $t_x = \frac{X}{X_n}$, $t_y = \frac{Y}{Y_n}$, and $t_z = \frac{Z}{Z_n}$, and where $X_N = 0.9642$, $Y_N = 1.0000$, and $Z_N = 0.8251$, the D65 white point coordinates are

$$f_i = \begin{cases} \sqrt{[3]}{t_i} & \text{if } t > \left(\frac{6}{29}\right)^3 \\ \frac{841t_i}{108} + \frac{4}{29} & \text{otherwise} \end{cases}$$

Smartphone Based-Image Acquisition. The code for analyzing ammonia concentrations was initially developed in MATLAB but can be easily adapted for integration into a smartphone application. It functions by capturing snapshots at predefined time intervals from user-recorded videos during the sensor-solution interaction. These snapshots are then cropped to the sensor's area of interest, and their average RGB values are computed and converted into the CIELAB color space to analyze changes in lightness and calculate the reaction growth rate. For concentration determination, the code uses the obtained reaction growth rate and applies the logistic function as explained in the main text. To maintain uniform lighting conditions for image analysis, we used a flash-light set at a consistent intensity level when capturing sensor photos.

■ ASSOCIATED CONTENT

Data Availability Statement

The data that support the findings of this study are available from the corresponding author upon reasonable request.

Supporting Information

The Supporting Information is available free of charge at https://pubs.acs.org/doi/10.1021/acsami.4c06615.

Supporting Information contains a full description of the XPS characterization of the samples (PDF)

■ AUTHOR INFORMATION

Corresponding Author

Debashis Chanda − *Department of Physics, University of Central Florida, Orlando, Florida 32816, United States; CREOL, The College of Optics and Photonics, University of Central Florida, Orlando, Florida 32816, United States; NanoScience Technology Center, University of Central Florida, Orlando, Florida 32826, United States*; Email: Debashis.Chanda@ucf.edu

Authors

Mahdi Soudi − *Department of Physics, University of Central Florida, Orlando, Florida 32816, United States; CREOL, The College of Optics and Photonics, University of Central Florida, Orlando, Florida 32816, United States; NanoScience Technology Center, University of Central Florida, Orlando, Florida 32826, United States*; orcid.org/0009-0002-0858-8577

Pablo Cencillo-Abad − *NanoScience Technology Center, University of Central Florida, Orlando, Florida 32826, United States*; orcid.org/0000-0002-4118-1560

Jay Patel − *NanoScience Technology Center, University of Central Florida, Orlando, Florida 32826, United States*

Suvash Ghimire − *Department of Materials Science and Engineering, University of Central Florida, Orlando, Florida 32816, United States*

Joseph Dillon − *NanoScience Technology Center, University of Central Florida, Orlando, Florida 32826, United States*

Aritra Biswas − *CREOL, The College of Optics and Photonics, University of Central Florida, Orlando, Florida 32816, United States; NanoScience Technology Center, University of Central Florida, Orlando, Florida 32826, United States*

Kausik Mukhopadhyay − *Department of Materials Science and Engineering and Advanced Materials Processing and Analysis Centre, University of Central Florida, Orlando, Florida 32816, United States*; orcid.org/0000-0001-9526-3791

Complete contact information is available at: https://pubs.acs.org/10.1021/acsami.4c06615

Notes

The authors declare no competing financial interest.

■ ACKNOWLEDGMENTS

This work at University of Central Florida was supported by National Science Foundation Grant #ECCS-1920840. We also want to acknowledge the Department of Homeland Security FEMA for a research assistantship to S.G. through Grant # EMW-2018-FP00329, and NSF MRI for XPS through NSF Grant# ECCS-1726636.

■ REFERENCES

(1) Babuji, P.; Thirumalaisamy, S.; Duraisamy, K.; Periyasamy, G. Human Health Risks Due to Exposure to Water Pollution: A Review. *Water* **2023**, *15* (14), 2532.

(2) Ryer-Powder, J. E. Health Effects of Ammonia. *Plant Oper. Progr.* **1991**, *10* (4), 228−232.

(3) Grove, G. L.; Duncan, S.; Kligman, A. M. Effect of Ageing on the Blistering of Human Skin with Ammonium Hydroxide. *Br. J. Dermatol.* **1982**, *107* (4), 393−400.

(4) Parvathy, A. J.; Das, B. C.; Jifiriya, M. J.; Varghese, T.; Pillai, D.; Rejish Kumar, V. J. Ammonia Induced Toxico-Physiological Responses in Fish and Management Interventions. *Rev. Aquacult.* **2023**, *15* (2), 452−479.

(5) Francis-Floyd, R.; Watson, C.; Petty, D.; Pouder, D. Ammonia in Aquatic Systems: FA-16/FA031, 06/2022. *EDIS* **2022**, *2022*(4)..

(6) Soler, P.; Faria, M.; Barata, C.; García-Galea, E.; Lorente, B.; Vinyoles, D. Improving Water Quality Does Not Guarantee Fish Health: Effects of Ammonia Pollution on the Behaviour of Wild-Caught Pre-Exposed Fish. *PLoS One* **2021**, *16* (8), No. e0243404.

(7) McGinn, S. M.; Janzen, H. H. Ammonia Sources in Agriculture and Their Measurement. *Can. J. Soil Sci.* **1998**, *78* (1), 139−148.

(8) Ammonia.Pdf. 2024, https://www.oregon.gov/oha/PH/HEALTHYENVIRONMENTS/DRINKINGWATER/MONITORING/Documents/health/ammonia.pdf (accessed June 12, 2024).

(9) Lin, K.; Zhu, Y.; Zhang, Y.; Lin, H. Determination of Ammonia Nitrogen in Natural Waters: Recent Advances and Applications. *Trends Environ. Anal. Chem.* **2019**, *24*, No. e00073.

(10) Kistemann, T.; Exner, M. Water Quality and Health Risks. *Understanding the Earth System: Compartments, Processes and Interactions*; Ehlers, E., Krafft, T., Eds.; Springer: Berlin, Heidelberg, 2001; pp 209−221.

(11) Li, D.; Xu, X.; Li, Z.; Wang, T.; Wang, C. Detection Methods of Ammonia Nitrogen in Water: A Review. *TrAC, Trends Anal. Chem.* **2020**, *127*, 115890.

(12) Ryu, H.; Thompson, D.; Huang, Y.; Li, B.; Lei, Y. Electrochemical Sensors for Nitrogen Species: A Review. *Sens. Actuators Rep.* **2020**, *2* (1), 100022.
(13) Smith, A. F.; Liu, X.; Woodard, T. L.; Fu, T.; Emrick, T.; Jiménez, J. M.; Lovley, D. R.; Yao, J. Bioelectronic Protein Nanowire Sensors for Ammonia Detection. *Nano Res.* **2020**, *13* (5), 1479−1484.
(14) Wang, C.; Wang, T.; Li, Z.; Xu, X.; Zhang, X.; Li, D. An Electrochemical Enzyme Biosensor for Ammonium Detection in Aquaculture Using Screen-Printed Electrode Modified by Gold Nanoparticle/Polymethylene Blue. *Biosensors* **2021**, *11* (9), 335.
(15) Al-Ammar, R. S. Urease Enzyme Biosensor for Water Pollution Detection. *Basrah J. Sci.* **2022**, *40* (3), 666−673.
(16) Mackin, C.; Schroeder, V.; Zurutuza, A.; Su, C.; Kong, J.; Swager, T. M.; Palacios, T. Chemiresistive Graphene Sensors for Ammonia Detection. *ACS Appl. Mater. Interfaces* **2018**, *10* (18), 16169−16176.
(17) Goldshleger, N.; Grinberg, A.; Harpaz, S.; Shulzinger, A.; Abramovich, A. Real-Time Advanced Spectroscopic Monitoring of Ammonia Concentration in Water. *Aquac. Eng.* **2018**, *83*, 103−108.
(18) Pérez-Sánchez, G. G.; Pinzón-Escobar, E. F.; Sandoval-Romero, G. E.; Chávez, J. A. Á. Erbium Doped Fiber Sensor for Ammonia Detection into Water. *J. Phys.: Conf. Ser.* **2015**, *582* (1), 012045.
(19) Leal-Junior, A. G.; Frizera, A.; Marques, C. High Sensitive Ammonia Detection in Water With Fabry-Perot Interferometers. *IEEE Photonics Technol. Lett.* **2020**, *32* (14), 863−866.
(20) Hossain, M. K.; Kitahama, Y.; Huang, G. G.; Han, X.; Ozaki, Y. Surface-Enhanced Raman Scattering: Realization of Localized Surface Plasmon Resonance Using Unique Substrates and Methods. *Anal. Bioanal. Chem.* **2009**, *394* (7), 1747−1760.
(21) Liu, Y.; Asset, T.; Chen, Y.; Murphy, E.; Potma, E. O.; Matanovic, I.; Fishman, D. A.; Atanassov, P. Facile All-Optical Method for In Situ Detection of Low Amounts of Ammonia. *iScience* **2020**, *23* (11), 101757.
(22) Timmer, B.; Olthuis, W.; Berg, A. v. d. Ammonia Sensors and Their Applications-a Review. *Sens. Actuators, B* **2005**, *107* (2), 666−677.
(23) Strömberg, N.; Hulth, S. An Ammonium Selective Fluorosensor Based on the Principles of Coextraction. *Anal. Chim. Acta* **2001**, *443* (2), 215−225.
(24) Tzollas, N. M.; Zachariadis, G. A.; Anthemidis, A. N.; Stratis, J. A. A New Approach to Indophenol Blue Method for Determination of Ammonium in Geothermal Waters with High Mineral Content. *Int. J. Environ. Anal. Chem.* **2010**, *90* (2), 115−126.
(25) Roth, M. Fluorescence Reaction for Amino Acids. *Anal. Chem.* **1971**, *43* (7), 880−882.
(26) Hu, H.; Liang, Y.; Li, S.; Guo, Q.; Wu, C. A Modified *o*-Phthalaldehyde Fluorometric Analytical Method for Ultratrace Ammonium in Natural Waters Using EDTA-NaOH as Buffer. *J. Anal. Methods Chem.* **2014**, *2014*, 1−7.
(27) Muniraj, S.; Yan, C.-T.; Shih, H.-K.; Ponnusamy, V. K.; Jen, J.-F. Determination of Ammonium in Aqueous Samples Using New Headspace Dynamic In-Syringe Liquid-Phase Microextraction with in Situ Derivitazation Coupled with Liquid Chromatography−Fluorescence Detection. *Anal. Chim. Acta* **2012**, *754*, 54−60.
(28) US EPA, O. EPA Method 350.1: Determination of Ammonia Nitrogen by Semi-Automated Colorimetry. 2023, https://www.epa.gov/esam/epa-method-3501-determination-ammonia-nitrogen-semi-automated-colorimetry (accessed Sept 15, 2023).
(29) Tittl, A.; Giessen, H.; Liu, N. Plasmonic Gas and Chemical Sensing. *Nanophotonics* **2014**, *3* (3), 157−180.
(30) Stewart, M. E.; Anderton, C. R.; Thompson, L. B.; Maria, J.; Gray, S. K.; Rogers, J. A.; Nuzzo, R. G. Nanostructured Plasmonic Sensors. *Chem. Rev.* **2008**, *108* (2), 494−521.
(31) Valsecchi, C.; Brolo, A. G. Periodic Metallic Nanostructures as Plasmonic Chemical Sensors. *Langmuir* **2013**, *29* (19), 5638−5649.
(32) Maier, S. A. *Plasmonics: Fundamentals and Applications*; Springer, 2007.
(33) Brolo, A. G. Plasmonics for Future Biosensors. *Nat. Photonics* **2012**, *6* (11), 709−713.
(34) Spackova, B.; Wrobel, P.; Bockova, M.; Homola, J. Optical Biosensors Based on Plasmonic Nanostructures: A Review. *Proc. IEEE* **2016**, *104* (12), 2380−2408.
(35) Zeng, S.; Baillargeat, D.; Ho, H.-P.; Yong, K.-T. Nanomaterials Enhanced Surface Plasmon Resonance for Biological and Chemical Sensing Applications. *Chem. Soc. Rev.* **2014**, *43* (10), 3426−3452.
(36) Vo-Dinh, T. M.; Fales, A. M.; Griffin, G. D.; Khoury, C.; Liu, Y.; Ngo, H. J.; Norton, S. J.; Register, J.; Wang, H.-N.; Yuan, H. Plasmonic Nanoprobes: From Chemical Sensing to Medical Diagnostics and Therapy. *Nanoscale* **2013**, *5* (21), 10127−10140.
(37) Prabhash, P. G.; Haritha, V. S.; Nair, S. S.; Pilankatta, R. Localized Surface Plasmon Resonance Based Highly Sensitive Room Temperature pH Sensor for Detection and Quantification of Ammonia. *Sens. Actuators, B* **2017**, *240*, 580−585.
(38) Amirjani, A.; Fatmehsari, D. H. Colorimetric Detection of Ammonia Using Smartphones Based on Localized Surface Plasmon Resonance of Silver Nanoparticles. *Talanta* **2018**, *176*, 242−246.
(39) Liu, Y.-N.; Chen, H.-B.; Liu, X.-W. Rapid Assessment of Water Toxicity by Plasmonic Nanomechanical Sensing. *Anal. Chem.* **2020**, *92* (1), 1309−1315.
(40) Zhou, T.; Zhang, P.; Yu, Z.; Tao, M.; Zhou, D.; Yang, B.; Zhang, T. Light-Driven, Ultra-Sensitive and Multifunctional Ammonia Wireless Sensing System by Plasmonic-Functionalized Nb2CTx MXenes towards Smart Agriculture. *Nano Energy* **2023**, *108*, 108216.
(41) Bothra, S.; Sahoo, S. K. Colorimetric Sensing Using Plasmonic Nanoparticles. *Sensing and Biosensing with Optically Active Nanomaterials*; Sahoo, S. K., Ed.; Micro and Nano Technologies; Elsevier, 2022; Chapter 7, pp 175−205.
(42) Soudi, M.; Darudi, A.; Soltani, P. Accurate Solution of the Transmission of Intensity Equation by the Hartmann on a Chip. In *Imaging and Applied Optics 2019 (COSI, IS, MATH, pcAOP) (2019), paper JW2A.43*; Optica Publishing Group, 2019.
(43) Samavati, Z.; Borhani, T. N.; Samavati, A.; Ismail, A. F.; Rahman, M. A.; Othman, M. H. D.; Soleymani, M. Optical Fiber Sensor Based on Magneto-Plasmonic Features of Ag-Co Nanostructure for Ppm Ammonium Detection in Aqueous Solutions. *Opt. Fiber Technol.* **2021**, *67*, 102730.
(44) Zhang, Q.; Chen, S.; Wang, H. A Surface Plasmon-Enhanced Nanozyme-Based Fenton Process for Visible-Light-Driven Aqueous Ammonia Oxidation. *Green Chem.* **2018**, *20* (17), 4067−4074.
(45) Quintanilla-Villanueva, G. E.; Maldonado, J.; Luna-Moreno, D.; Rodríguez-Delgado, J. M.; Villarreal-Chiu, J. F.; Rodríguez-Delgado, M. M. Progress in Plasmonic Sensors as Monitoring Tools for Aquaculture Quality Control. *Biosensors* **2023**, *13* (1), 90.
(46) Cencillo-Abad, P.; Mastranzo-Ortega, P.; Appavoo, D.; Guo, T.; Zhai, L.; Sanchez-Mondragon, J.; Chanda, D. Reusable Structural Colored Nanostructure for Powerless Temperature and Humidity Sensing. *Adv. Opt. Mater.* **2023**, *11*, 202300300R1.
(47) Franklin, D.; He, Z.; Mastranzo Ortega, P.; Safaei, A.; Cencillo-Abad, P.; Wu, S.-T.; Chanda, D. Self-Assembled Plasmonics for Angle-Independent Structural Color Displays with Actively Addressed Black States. *Proc. Natl. Acad. Sci. U.S.A.* **2020**, *117* (24), 13350−13358.
(48) Soudi, M.; Cencillo-Abad, P.; Chanda, D. Plasmonic Structural Color-Based Sensors. In *Advanced Fabrication Technologies for Micro/Nano Optics and Photonics XVII*; SPIE, 2024; Vol. *PC12898*, p PC128980B.
(49) Cencillo-Abad, P.; Franklin, D.; Mastranzo-Ortega, P.; Sanchez-Mondragon, J.; Chanda, D. Ultralight Plasmonic Structural Color Paint. *Sci. Adv.* **2023**, *9* (10), No. eadf7207.
(50) Malacara, D. *Color Vision and Colorimetry: Theory and Applications*, 2nd ed.; SPIE Press, 2011.
(51) Tsoularis, A.; Wallace, J. Analysis of Logistic Growth Models. *Math. Biosci.* **2002**, *179* (1), 21−55.
(52) Cencillo-Abad, P.; McCormack, S.; Guo, T.; Biswas, A.; Chanda, D. Angle- and Polarization-Independent Structural Color Based on Controlled Phase and Gain Margins in Ultrathin Transparent Dielectrics. *ACS Photonics* **2023**, *10* (8), 2909−2917.

https://doi.org/10.1021/acsami.4c06615
ACS Appl. Mater. Interfaces XXXX, XXX, XXX−XXX